

NASA Technical Memorandum 102088

# Fundamental Tribological Properties of Ion-Beam-Deposited Boron Nitride Films

Kazuhisa Miyoshi  
*Lewis Research Center*  
*Cleveland, Ohio*

October 1989

**NASA**

(NASA-TM-102088) FUNDAMENTAL TRIBOLOGICAL  
PROPERTIES OF ION-BEAM-DEPOSITED BORON  
NITRIDE FILMS (NASA) 25 p CSCL 11C

N90-11881

Unclas  
63/27 0239285



# FUNDAMENTAL TRIBOLOGICAL PROPERTIES OF ION-BEAM-DEPOSITED BORON NITRIDE FILMS

Kazuhisa Miyoshi  
National Aeronautics and Space Administration  
Lewis Research Center  
Cleveland, Ohio 44135

## ABSTRACT

The adhesion, friction, and micromechanical properties of ion-beam-deposited boron nitride (BN) films are reviewed in this chapter. The BN films are examined in contact with BN, metals, and other harder materials. For simplicity of discussion, the tribological properties of concern in the processes are separated into two parts. First, the pull-off force (adhesion) and the shear force required to break the interfacial junctions between contacting surfaces are discussed. The effects of surface films, hardness of metals, and temperature on tribological response with respect to adhesion and friction are considered. The second part deals with the abrasion of the BN films. Elastic, plastic, and fracture behavior of the BN films in solid-state contact are discussed. The scratch technique of determining the critical load needed to fracture interfacial adhesive bonds of BN films deposited on substrates is also addressed.

## INTRODUCTION

The technical function of numerous engineering systems such as machines, instruments, and vehicles depends on processes of motion. According to its basic physical definition, the term "motion" denotes the change in the position of an object with time. Many processes in nature and technology depend on the motion and dynamic behavior of solids, liquids, and gases.

Tribology is "the science and technology of interacting surfaces in relative motion and of associated subjects and practices" [1]. Tribology deals with force transference between surfaces moving relative to each other and includes such subjects as adhesion, friction, wear, and lubrication. Mechanical systems such as bearings, gears, and seals are examples of components involving tribology. The function of tribological research is to bring about a reduction in the adhesion, friction, and wear of mechanical components, to prevent their failure and to provide long, reliable component life through the judicious selection of materials, operating parameters, and lubricants.

Ceramic materials are being used increasingly for machine elements in sliding or rolling contact. These elements include components of advanced engines, such as bearings, seals, and gears, and tools used in metal shaping, such as cutting tools and extrusion dies. The successful use of ceramics in these applications is limited more often by tribological problems than by material properties or processing deficiencies [2-5]. Clearly, there is a great need for a fundamental understanding of the surface interactions of ceramics with ceramics and other materials [6].

Monolithic ceramics continue to be of great interest for structural use in automobile and aerospace engines because of such properties as high-temperature strength, environmental resistance, and low density. However, the severity of operating conditions in engines has not favored the use of bulk ceramics because of their high sensitivity to

microscopic flaws and catastrophic fracture behavior. This brittle nature translates into low reliability for ceramic components and, thus, limited application in engines [7-9].

For safety in critical automobile and aerospace applications, the components are required to display markedly improved toughness and noncatastrophic, or graceful, fracture [7-9]. Thus, the enhanced interest in ceramic materials has been further expanded to include high-performance ceramic-coated materials and fiber-reinforced ceramics.

Thin ceramic films are widely used in a variety of applications in which materials in monolithic form are not suitable because of diverse and special requirements. Also, thin ceramic films serve a variety of purposes: providing resistance to abrasion, erosion, corrosion, wear, radiation damage, or high-temperature oxidation; reducing adhesion and friction; and providing lubrication [10-14].

Boron nitride (BN) is a promising ceramic material for use as a high-temperature, wear resistant, hard solid lubricating film as well as a protective insulator film on semiconductors under a variety of environmental conditions [15-18].

Boron nitride can be deposited by a variety of techniques, including ion beam deposition [19,20], low-temperature chemical vapor deposition [21,22], plasma deposition [23,24], radiofrequency glow discharge [25], sputtering [26], borazine pyrolysis [27], and others [28]. The strength and durability of the films depend largely on the interfacial adhesive bond formed between the film and the substrate.

The objective of this chapter is to review the author's research of fundamental tribological properties and micromechanical properties of ion-beam-deposited BN films on metallic and nonmetallic substrates. Some earlier publications on this research are given in references 29 to 31.

First, the surface chemistry, microstructure, and bulk chemical composition of the BN films were investigated. Second, the BN films were brought into contact with BN, metals, and other harder materials to examine the tribological properties of the materials. For simplicity of discussion, the tribological properties of concern in the processes are separated into two parts.

First, the pull-off force (adhesion) and the shear force required to break the interfacial junctions between contacting surfaces are discussed. The effects of surface contaminant films, hardness of metals, and temperature on tribological response with respect to adhesion and friction are considered.

The second part deals with the abrasion of BN films. Elastic, plastic, and fracture behavior of BN films in solid-state contact are discussed. The scratch technique of determining the critical load needed to fracture interfacial adhesive bonds of ceramics deposited on substrates is also addressed.

## ION-BEAM-DEPOSITED BORON NITRIDE

Thin films containing BN have been synthesized by using an ion beam extracted from a borazine ( $B_3N_3H_6$ ) plasma [20]. The substrates used were both metallic and nonmetallic materials. The metallic substrates were 440C stainless steel, 304 stainless steel, and titanium (99.97 percent pure). The nonmetallic substrates were silicon, quartz (fused silica,  $SiO_2$ ), gallium arsenide (GaAs), and indium phosphide (InP) (table I). The BN films on the metallic substrates were approximately 2  $\mu m$  thick, and those on the nonmetallic substrates were 0.2  $\mu m$  thick (table I).

### Boron Nitride Surface

X-ray photoelectron spectroscopy (XPS) survey spectra of the BN film surfaces on the substrates obtained before sputter cleaning typically revealed a carbon peak as well as an adsorbed oxygen peak, as shown by curves (a) in figure 1 [29,30]. A layer of adsorbate on the surface consisted of water vapor and hydrocarbons from the atmospheric environment that may have condensed and become physically adsorbed to the BN film. After BN film surfaces had been sputter cleaned with argon ions for 45 min, small carbon and oxygen contamination peaks as well as the boron and nitrogen remained (curves (b) in fig. 1).

The  $B_{1s}$  photoelectron emission lines of the BN (fig. 1) peaked primarily at 190 eV, which is associated with BN. They also included a small amount of boron carbide ( $B_4C$ ). The  $N_{1s}$  photoelectron lines for the BN peaked primarily at 397.9 eV, which is again associated with BN. The  $C_{1s}$  photoelectron lines taken from the as-received surface at 284.6 eV indicate the presence of adventitious adsorbed carbon contamination with a small amount of carbides. After sputter cleaning, the adsorbed carbon contamination peak disappeared from the spectrum, and the relatively small carbide peak could be seen. The  $O_{1s}$  photoelectron lines of the as-received BN surface peaked at 531.6 eV because of adsorbed oxygen contamination and oxides. After sputter cleaning, the adsorbed oxygen contamination peak disappeared from the spectrum, but the small oxide peak remained.

TABLE I.—NONMETALLIC SUBSTRATES AND BN FILM THICKNESS

(a) Nonmetallic substrates

Material	Doping		Resistivity, $\Omega$ -cm	Sliding		Primary cleavage plane
	Dopant	Concentration, $\text{cm}^{-3}$		Plane	Direction	
Si	---	-----	0.01 to 0.02	{100}	<110>	{111}
SiO <sub>2</sub> (quartz)	---	-----	-----	---	---	---
<i>p</i> -type GaAs	Zn	$3 \times 10^{17}$	0.12	{100}	<110>	{110}
<i>n</i> -type GaAs	Te	$3 \times 10^{17}$	-----	↓	↓	↓
InP	---	-----	-----	↓	↓	↓
<i>n</i> -type InP	Sn	$3 \times 10^{17}$	0.010	↓	↓	↓

(b) BN film thickness for nonmetallic substrates

Substrate and film	BN film thickness, <sup>a</sup> nm
Si coated with BN at 200 °C	169.7 ± 4.4
Si coated with BN at 350 °C	118.3 ± 0.7
SiO <sub>2</sub> coated with BN at 200 °C	-----
SiO <sub>2</sub> coated with BN at 350 °C	-----
Zn-doped, <i>p</i> -type GaAs coated with BN	-----
Te-doped, <i>n</i> -type GaAs coated with BN	129.0
InP coated with BN	-----
Sn-doped, <i>n</i> -type InP coated with BN	116.0 ± 0.5

<sup>a</sup>Film thicknesses were determined by using a rotating analyzer ellipsometer with a helium-neon laser, a mercury arc lamp, or a xenon arc lamp as light sources.

The peak intensity for both boron and nitrogen associated with BN increased with argon ion sputter cleaning; that for carbon and oxygen decreased markedly. The BN film deposited on the 440C substrate was nonstoichiometric, with a boron-to-nitrogen (B/N) ratio of 1.6.

### Microstructure and Bulk Composition

The ion-beam-deposited BN films were hard and semitransparent. For example, figure 2 presents a microstructural appearance of a 304 stainless steel substrate coated with the 2- $\mu$ m-thick BN film under an optical microscope. The surface hardness of the ion-beam-deposited BN films is presented later in the section Micromechanical Properties.

A typical transmission electron photomicrograph (fig. 3(a)) indicates that the BN film lacked the macroscopic structural features common in both the monolithic cubic and hexagonal forms of BN [30]. In the absence of macroscopic crystallinity neither grains, grain boundaries, grain orientations, nor additional phases were found to exist. The electron diffraction pattern of the film (fig. 3(b)) indicates a diffused ring structure containing three rings that were identified as hexagonal (BN)<sub>4</sub>H. This evidence suggests the presence of, in addition to a structureless amorphous phase, a

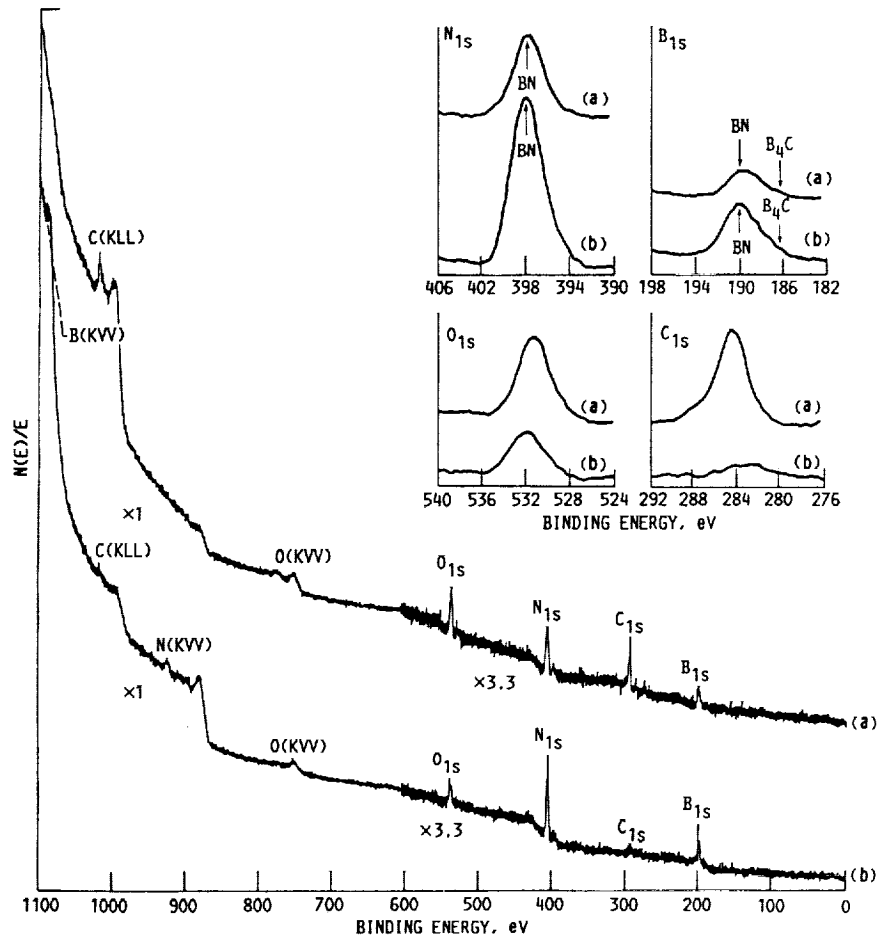
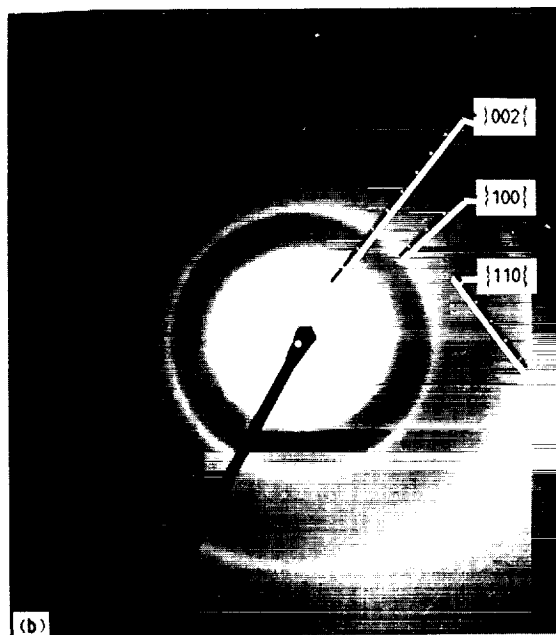
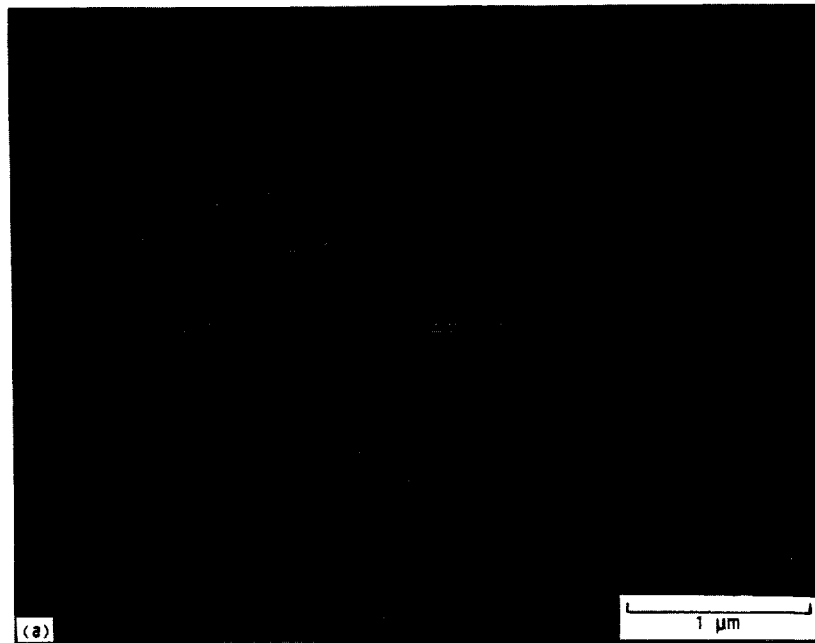


Figure 1.—X-ray photoelectron spectroscopy (XPS) spectra of ion-beam-deposited BN film before and after ion sputtering, curves (a) and (b), respectively (sputtering time, 45 min; substrate, 440C stainless steel).



Figure 2.—Microstructural appearance of 304 stainless steel coated with ion-beam-deposited BN films as observed through BN film under optical microscope.



(a) Transmission electron micrograph.  
 (b) Electron diffraction pattern.

Figure 3.—Typical microstructure and electron diffraction pattern of BN coating film.

crystalline phase with a size range of 8 to 30 nm (i.e., the films were not completely amorphous; properties characteristic of hexagonal BN were detected). This finding agrees with electron microscopical and optical band gap observations [17,18].

Elemental depth profiles for the ion-beam-deposited BN film on silicon were obtained as a function of the sputtering time from Auger electron spectroscopy (AES) analyses by Pouch (fig. 4) [18]. The height of the boron and nitrogen peaks rapidly increased with an increase in the sputtering time. The oxygen and carbon peaks, however, decreased in the first 1 to 2 min and remained constant thereafter. The BN film deposited on silicon had a B/N ratio of about 2. Thus XPS and AES analyses clearly revealed that BN was nonstoichiometric and that small amounts of oxides and carbides were present on the surface and in the bulk of the BN film. Contaminants such as carbides (e.g.,  $B_4C$ ) and oxides may be introduced and absorbed in the BN film during ion beam deposition.

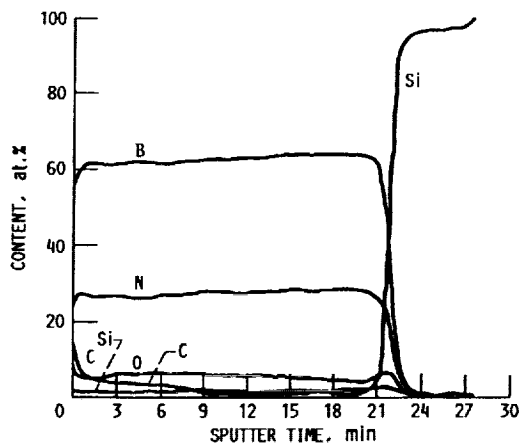


Figure 4.—Auger electron spectroscopy (AES) depth profile; atomic percent as function of sputter time for ion-beam-deposited BN film on Si (deposition temperature, 200 °C; ion beam energy, 150 eV).

The BN films deposited on the silicon substrates were probed by using secondary ion mass spectroscopy by Pouch [18]. The spectra indicated the presence of the following secondary ions:  $B^+$ ,  $B_2^+$ ,  $C^+$ ,  $O^+$ ,  $Si^+$ ,  $Si_2^+$ , and  $SiO^+$ . The peak observed at 14 amu could result from  $N^+$ ,  $CH_2^+$ , and  $SiO_2^+$ . Additional peaks at 24 and 25 amu were related to  $BN^+$  and thus supported the XPS data. The  $SiO^+$  signal was associated with the oxide present at the BN-to-silicon interface.

## ADHESION AND FRICTION

### Clean and Contaminated Surfaces

The surfaces of ceramics and metals usually contain, in addition to the constituent atoms, adsorbed films of water vapor or hydrocarbons that may have condensed from the environment.

In a vacuum environment, sputtering with rare gas ions or heating surfaces to very high temperatures can remove contaminants that are adsorbed on the surface of ceramics and metals. Removing adsorbed films from these surfaces results in very strong interfacial adhesion when two such solids are brought into contact. Typical adhesion results from ion-beam-deposited BN film in contact with a monolithic magnesia-doped silicon nitride ( $Si_3N_4$ ) are presented in figure 5. The  $Si_3N_4$  pins were sputter cleaned with argon before adhesion experiments. The surfaces of BN films were in two states: as-received and heat cleaned at 700 °C. The strength of adhesion is expressed as the force

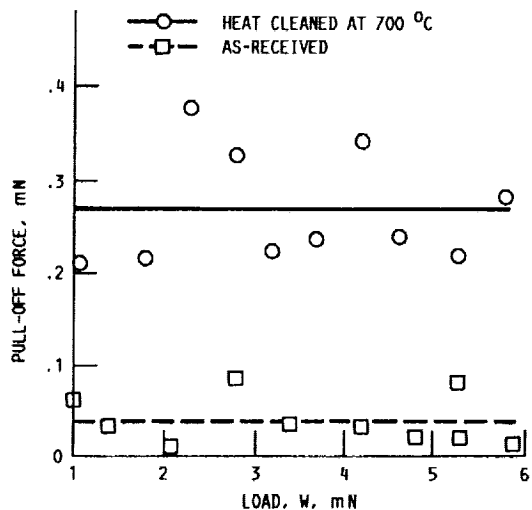


Figure 5.—Pull-off force (adhesion) as function of load for ion-beam-deposited BN films in contact with hemispherical monolithic  $Si_3N_4$  pins at room temperature in vacuum.

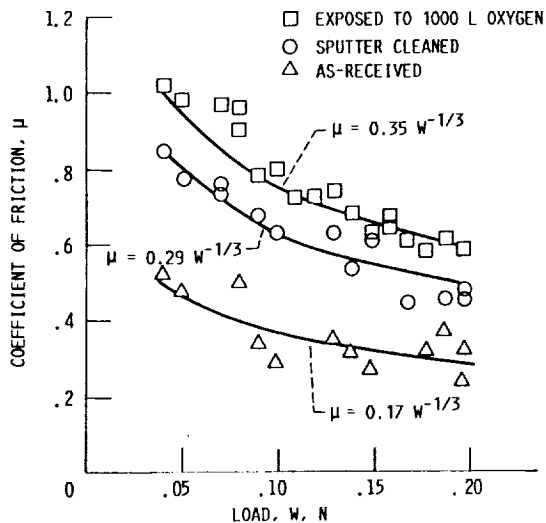


Figure 6.—Coefficient of friction as function of load for hemispherical BN pins in sliding contact with BN flats (single-pass sliding; sliding velocity, 3 mm/min; vacuum, 30 nPa; room temperature;  $L = 1 \times 10^{-6}$  torr·sec).

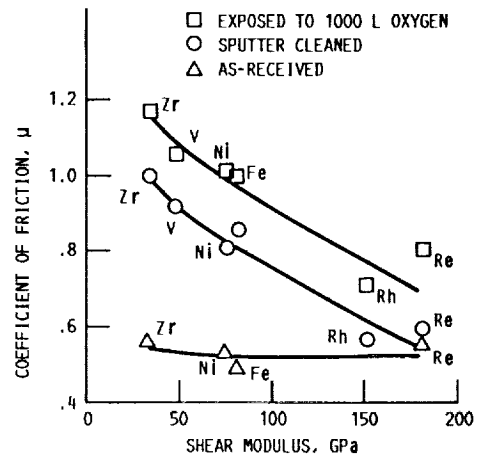


Figure 7.—Coefficient of friction as function of shear modulus of metals in contact with BN flats (single-pass sliding; sliding velocity, 3 mm/min; vacuum, 30 nPa; room temperature,  $L = 1 \times 10^{-6}$  torr·sec).

necessary to pull the surfaces apart; it is called the pull-off force [32]. The plots indicate no significant change in the pull-off force with respect to load over the light load range of 1 to 6 mN. The data, however, indicate clearly that the contaminants on the BN surfaces greatly reduce the extent of adhesion (by about a factor of 7).

Figures 6 and 7 present typical plots of the coefficients of friction for the ion-beam-deposited BN films in contact with BN and with metals, respectively. The surfaces of BN films and metals were in three states: as received, argon ion sputter cleaned, and exposed to 1000 L ( $L = 1 \times 10^{-6}$  torr·sec) of oxygen with an oxygen pressure of  $1 \times 10^{-6}$  torr after sputter cleaning. The coefficients of friction are strongly affected by contaminants adsorbed on the as-received surfaces. The coefficients of friction for the sputter-cleaned surfaces are higher than those for the as-received surfaces. In other words, the presence of the contaminants on the as-received surface of the BN film reduces the adhesion and shear strength of the contact area.

In contrast, oxygen exposures to clean BN and metal surfaces strengthen the BN-to-BN adhesion and metal-to-BN adhesion (figs. 6 and 7). It is known that exposing both metal and ceramic surfaces to oxygen under carefully controlled conditions, after sputtering with argon ions or heating in vacuum, results in the adsorption of oxygen, which produces the following two effects: (1) The metal and ceramic oxidize and form an oxide surface layer; and (2) the oxide layers increase the shear strength of the contact and the coefficients of friction [33,34]. In these cases strong oxide-to-oxide bonding takes place at the interfaces, thereby raising the shear strength and the coefficient of friction.

Figure 6 also indicates that adhesion and friction for BN-to-BN contacts decrease as the load increases under all three surface conditions. Further, figure 7 indicates that adhesion and friction for sputter-cleaned metal-to-BN couples are smaller for metals with a large shear modulus. These subjects are discussed in somewhat greater detail in the following sections.

### Area of Contact

Boron nitride films behave elastically up to a certain contact pressure. For example, when BN coated on a 440C bearing stainless steel flat is placed in contact with BN on a 440C stainless steel pin in a vacuum, the coefficient of friction is not constant. It decreases as the load increases, as shown in figure 6. To a first approximation for the load range investigated, the relation between coefficient of friction  $\mu$  and load  $W$  on logarithmic coordinates is given by the expression

$$\mu = kW^{-1/3} \quad (1)$$

The exponent arises from an adhesion mechanism for the surfaces in solid-state contact. The area of elastic contact can be determined by the elastic deformation [35]. The friction is found to be a function of the shear strength of this elastic contact area. Similar contact and friction characteristics for diamond on diamond and diamond on silicon carbide were also found [35,36].

The data of figure 7, for surfaces sputter-cleaned with argon ions, indicate a decrease in coefficient of friction with an increase in shear modulus of the metals. Note that the magnitude of shear modulus, like Young's modulus, is generally dependent on the electron configuration of the metal [37]; its maximum value in a given period of the periodic table corresponds to the metal having the maximum number of unpaired *d* electrons. The minimum near the end of each period occurs for the element that has an  $s^2p^1$  configuration. Shear and Young's moduli are also related to such physical, chemical, and mechanical properties as surface and cohesive energy, chemical stability, and tensile and shear strength [37-41]. Further, all the slidings in this investigation involve adhesion at the contact area between the metal and BN.

The morphology revealed that all the BN surfaces contacted by the metals contained transferred films of metal. On separation of the BN and metal in sliding contact, both the interfacial adhesive bonds between the metal and BN and the cohesive bonds in the metal were broken. In other words, the shear forces that broke both the interfacial adhesive bonds and the cohesive bonds in the metal were primarily responsible for the frictional force. The examined metal failed in shear or tension at some of the real areas of contact where the interfacial bonds were stronger than the cohesive bonds in the metal. Metals that have a low shear modulus exhibit larger areas of metal transfer than those with a high modulus. Such dependence of friction and metal transfer on shear modulus may arise from surface and cohesive energy as well as from ductility of the metals; therefore, it is interesting to compare the foregoing friction results, for metal-to-BN contacts, with surface energy and hardness of metals.

Figure 8 presents surface energy values at room temperature from recommended values suggested by Tyson and Miedema [38,40]. The surface energy for the metals increases with an increase in shear modulus. Note that Miedema [40] estimated the values at room temperature from values of the experimental surface energy and entropy by using temperature dependence factors. The surface energy is correlated with such thermochemical parameters for metals as electron density, electron negativity, and heat sublimation [39,40]. The calculated ideal shear strengths of the metals were also correlated with shear modulus [41]—the higher the shear modulus, the greater the shear strength.

The adhesion and friction of the metal-to-BN contacts were expected to increase as the surface energy (i.e., the bond energy of metals) increased. But figures 7 and 8 show that the adhesion and friction go in the opposite direction; they decreased with an increase in surface energy of metals. In other words, the friction was reduced with an increase in shear modulus, whereas the surface energy increased as the modulus value increased. Presumably, the ductility of metals, that is, the deformation of metals, has not been considered here [42,43].

Because of the marked difference in elastic and plastic deformation of ceramics and softer metals, solid-state contact between the two materials can result in considerable plastic deformation of the softer metal. This deformation can contribute to the adhesion and friction of the materials because it increases the real contact area. To gain an understanding of interface deformation under the action of a friction force, indentation experiments were conducted with the metal pin specimens. The hardness data (fig. 9(a)) indicate that at room temperature the Vickers hardness of metals increases as the shear modulus increases. Figure 9(b) presents areas of contact, calculated from the experimental data presented in figure 9(a), as a function of shear modulus of the metal. The area of contact was determined by the ratio of normal load to hardness. The calculated area of contact is very strongly dependent on the shear modulus of the metal; it decreases with increasing shear modulus. The decrease in the area of contact with an increase of shear modulus for these metals is greater than the corresponding increase in the surface energy (bond energy) with shear modulus. (See figs. 8 and 9(b).) Consequently, the shear force required to move the metal pin in a direction parallel to the surface of BN decreases with increasing shear modulus. This fact is consistent with the results shown in figure 7. Thus, such mechanical factors as hardness are of great importance [42,43]. During ceramic-to-metal contact, strong bonds form between the materials. These interfacial bonds are stronger than the cohesive bonds in the metal (as evidenced by the transferred metal) at the major part of the real area of contact. Hardness of metals plays an important role in adhesion and friction and exceeds that of the surface energy.

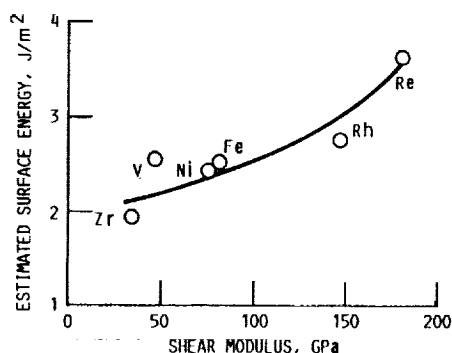


Figure 8.—Estimated surface energy of metal as function of shear modulus.

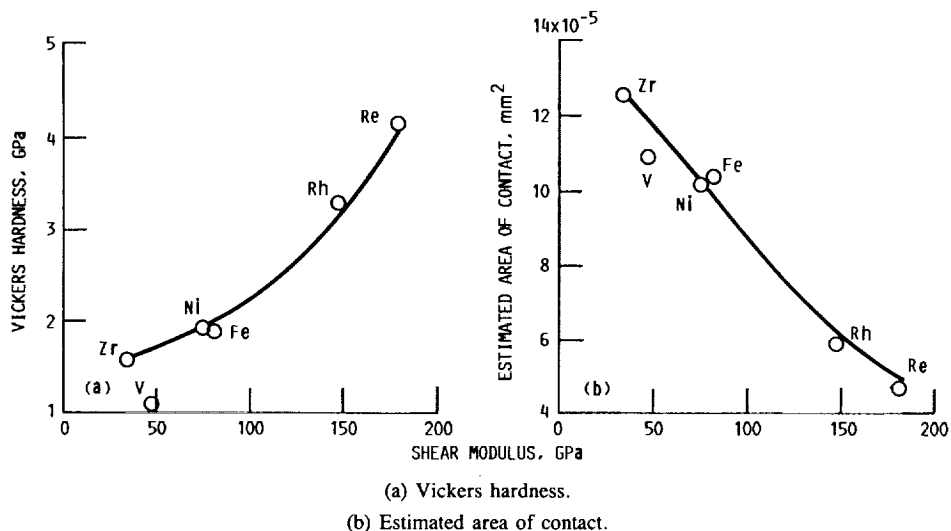


Figure 9.—Vickers hardness of metals and estimated area of contact as functions of shear modulus.

### Temperature Effects

An increase in surface temperature of a ceramic material tends to promote surface chemical reactions. These chemical reactions cause products to appear on the surface which can alter tribological behavior [44].

Figure 10 presents the average pull-off forces (adhesion) for the BN films at 700 °C in vacuum as a function of temperature. The BN films were heat cleaned at 700 °C in vacuum, and the monolithic Si<sub>3</sub>N<sub>4</sub> pins were sputter cleaned with argon ions before adhesion experiments.

Although the pull-off force for the BN films increased slightly with temperatures up to 400 °C, it generally remained low at these temperatures. The pull-off force increased significantly at 500 °C and remained high, in the range of 500 to 700 °C. Strong adhesive bonding resulting from a strong chemical reaction between the BN film and monolithic Si<sub>3</sub>N<sub>4</sub> can take place at the contacting interface at temperatures in the range of 500 to 700 °C.

In general, the behavior of pull-off force (adhesion) is primarily related to that of static and dynamic friction in vacuum [45].

### Comparison of Coefficients of Friction

Figure 11 summarizes friction properties for ceramic-to-ceramic, metal-to-metal, and metal-to-ceramic contacts in vacuum environments. In addition to the BN coating, ceramics of concern include SiC, Si<sub>3</sub>N<sub>4</sub>, SiO<sub>2</sub>, and ferrite

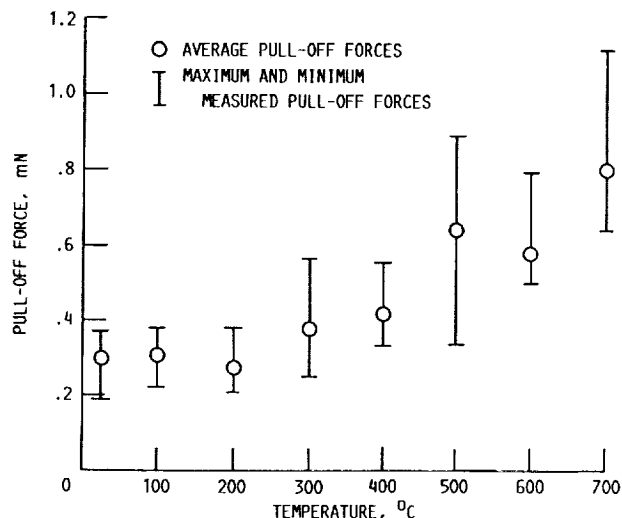


Figure 10.—Pull-off force (adhesion) as function of temperature for ion-beam-deposited BN films in contact with hemispherical monolithic Si<sub>3</sub>N<sub>4</sub> pins in vacuum.

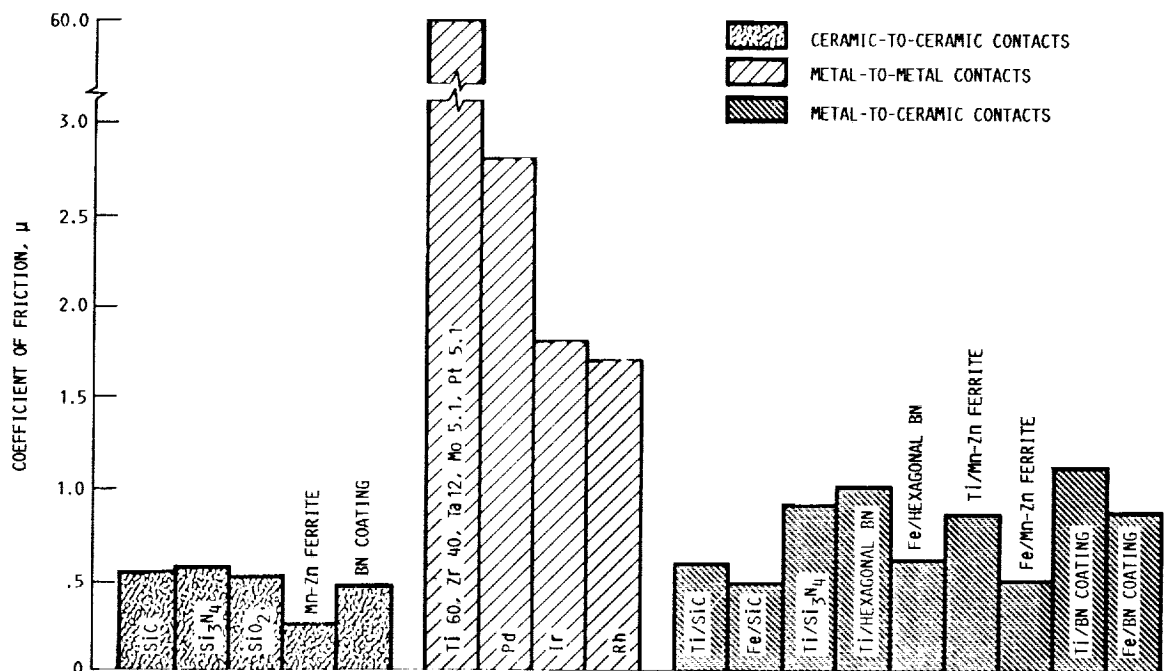


Figure 11.—Coefficients of friction for clean solid-to-solid interfaces (single-pass sliding; vacuum, 30 nPa).

in bulk form. Metals of concern include titanium, zirconium, tantalum, molybdenum, platinum, palladium, iridium, rhodium, and iron.

The data presented in figure 11 indicate the marked difference in friction for the combination of clean solids. The coefficients of friction due to adhesive bonding for ceramic-to-ceramic and metal-to-ceramic contacts were much lower than those for metal-to-metal contacts. The coefficients of friction for metal-to-metal contacts were extremely high. In general, the coefficient of friction for BN-to-BN contact can fit into the category of ceramic-to-ceramic contact. The coefficient of friction for metal-to-BN contact can fit into the category of metal-to-ceramic contact.

Figure 11 suggests that the use of ceramic materials, including bulk and coatinglike forms, in vacuum, spacelike environments is beneficial from tribological considerations.

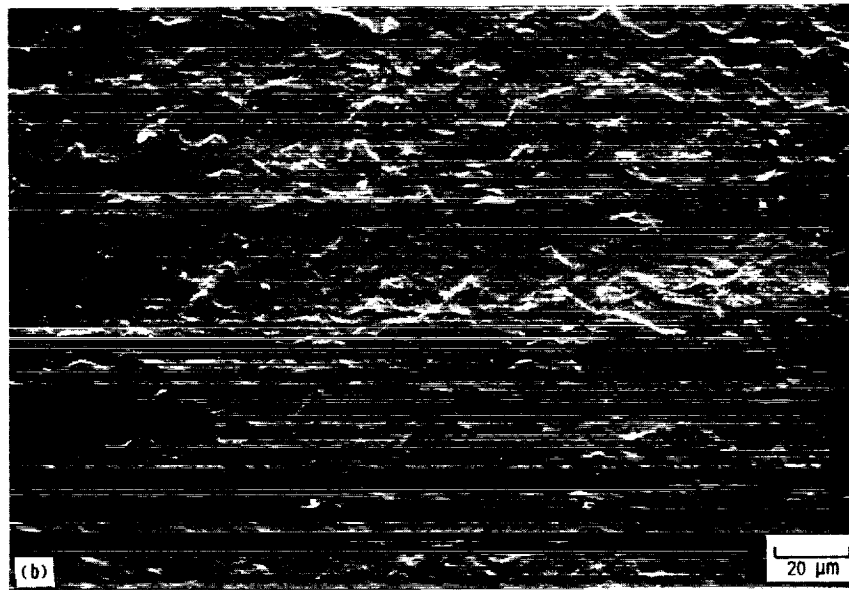
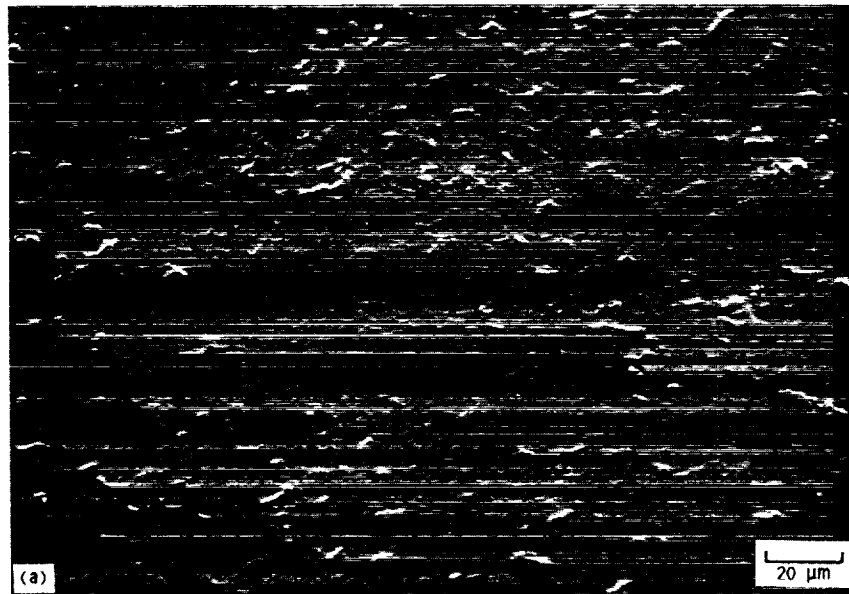
## MICROMECHANICAL PROPERTIES

Ceramics, in both coating and monolithic form, behave micromechanically in a ductile fashion to a certain contact stress when they are brought into contact with ceramics or other solids. Even at room temperature, ceramics such as BN and SiC behave elastically and plastically at low stresses under relatively modest conditions of rubbing contact; however, they microfracture under more highly concentrated contact stresses [30,31,36,46–50]. This microfracture, known as brittle fracture, is one of the most critical characteristics of a ceramic that must be considered in design for structural and tribological applications.

Single-pass scratch experiments were conducted to examine the deformation and fracture behavior of BN films sliding against a 0.2-mm-radius diamond pin in air at a relative humidity of 45 percent and at room temperature [30,31]. The BN films were deposited on both metallic and nonmetallic substrates.

### Elasticity

When a BN film surface is brought into sliding contact with a diamond under relatively small load (< 2 N), elastic deformation can occur locally in both the BN film and the diamond. Sliding occurs at the interface. The coefficient of friction was not constant and decreased as the load increased. The friction characteristics were similar to those for BN-to-BN contacts presented earlier in figure 6. In these experiments no permanent groove formation due to plastic flow and no cracking of the BN film with sliding were observed [31].



(a) 440C stainless steel substrate.  
 (b) Titanium substrate.

Figure 12.—Scanning electron photomicrographs of wear tracks on BN film surfaces generated by 0.2-mm-radius diamond pins (load, 4N; sliding velocity, 12 mm/min; laboratory air).

### Plasticity

An increase (of a few newtons) in load results in plastic deformation of the BN film, as shown in figure 12. The spherical diamond indented and slid on the BN film without suffering permanent deformation, but it caused permanent grooves in the BN film during sliding. The BN film deformed plastically much like metallic films. Scratch measurements were therefore conducted with BN films deposited on the metallic and nonmetallic substrates, starting from the smallest loads at which the scratches were visible by optical and scanning electron microscopy and detectable by surface profilometry.

The width  $D$  and height  $H$  of a groove with some amount of deformed BN piled up along its sides are defined in figure 13. The widths of the grooves reported herein were obtained by averaging the widths from 10 or more measurements of surface profile traces, and by optical or scanning electron microscope examinations.

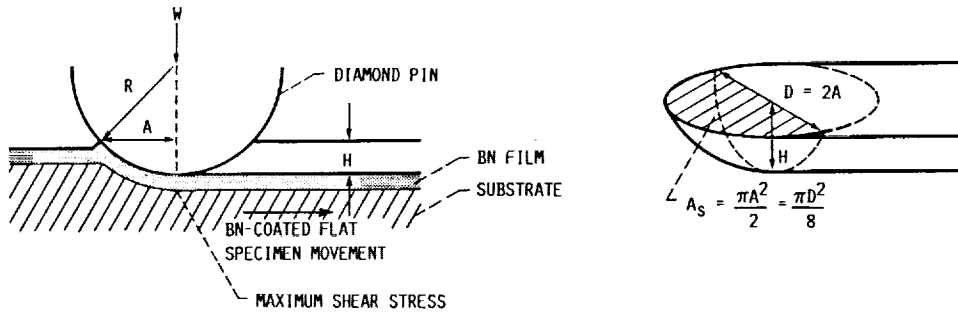
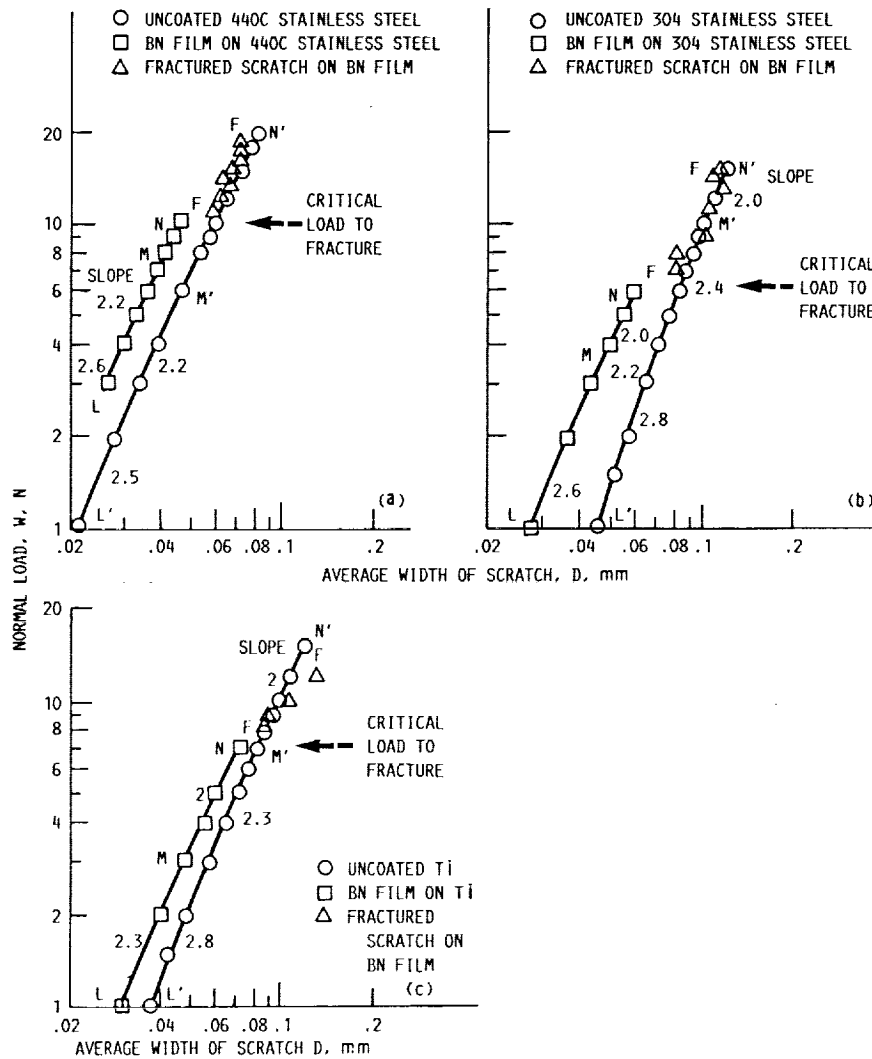


Figure 13.—Definition of mean contact pressure ( $P = W/A_s$ ).

The relationship between the load and the width of the resulting scratch may be expressed with a number of empirical relations [51]. When the average scratch width  $D$  for BN films is plotted as a function of the load  $W$  on logarithmic coordinates, this is expressed as  $W = kD^n$  (i.e., Meyer's law, as typically presented in figures 14 and 15).

Figures 14 and 15 present data for scratch widths obtained for BN films on 440C stainless steel, 304 stainless steel, and titanium substrates and on silicon,  $\text{SiO}_2$ , GaAs, and InP substrates, respectively. Comparative data for

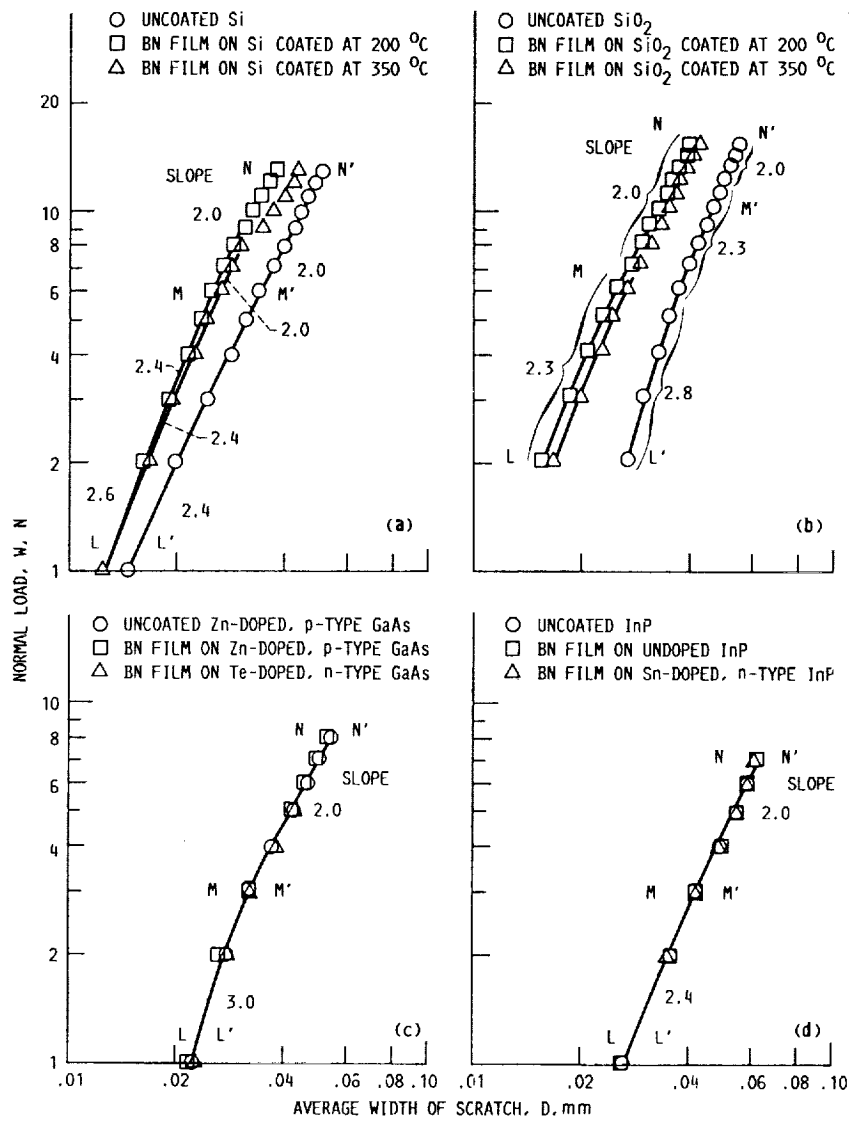


(a) BN film on 440C stainless steel and uncoated 440C stainless steel.

(b) BN film on 304 stainless steel and uncoated 304 stainless steel.

(c) BN film on Ti and uncoated Ti.

Figure 14.—Scratch width as function of load for metallic substrates (sliding velocity, 12 mm/min; laboratory air; portion FF represents fractured scratch on BN film).



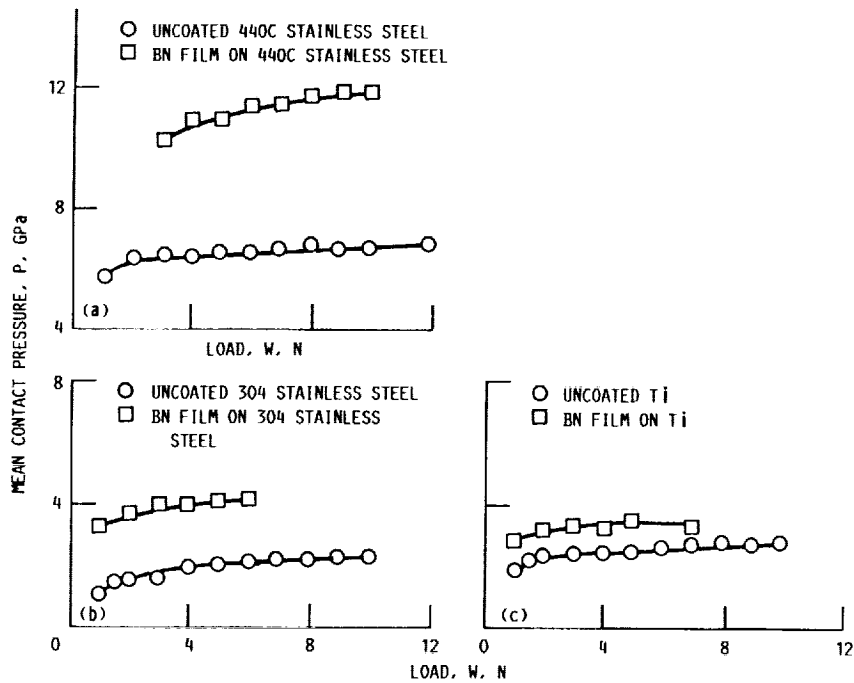
(a) BN film on Si and uncoated Si.  
 (b) BN film on SiO<sub>2</sub> and uncoated SiO<sub>2</sub>.  
 (c) BN film on GaAs and uncoated GaAs.  
 (d) BN film on InP and uncoated InP.

Figure 15.—Scratch width as function of load for nonmetallic substrates (sliding velocity, 12 mm/min; laboratory air).

uncoated 440C stainless steel, 304 stainless steel, titanium, silicon, SiO<sub>2</sub>, GaAs, and InP are also presented in figures 14 and 15. The portion LM for BN films or L'M' for uncoated material is gradually curved but is considered to be composed of approximately straight portions of transitional slopes. For example, the transitional slopes are 2.6 and 2.2 for BN film on 440C stainless steel, and 2.6 and 2.4 for BN film on silicon.

The portion MN for BN films or M'N' for uncoated materials is a straight line of slope 2. It is evident that MN or M'N' is the range over which Meyer's law is valid for BN films on both metallic and nonmetallic substrates as well as for uncoated metallic and nonmetallic materials. Here the Meyer's index  $n$  is a constant and has a value of 2. Thus, the BN films on both metallic and nonmetallic substrates behave plastically much like metals when they are brought into sliding contact with hard solids such as diamond.

It is interesting that in figure 14 the portion FF, representing the condition of fracture where the load exceeds the critical load, is also roughly expressed by  $W = kD^n$ . The fractured scratch in the BN film on the substrate is almost as wide as the scratch in the uncoated metallic material used for the substrate. This evidence confirms that cracks are generated from the contact area rather than from the free surface of the film. It suggests that the substrate is responsible not only for controlling the critical load which will fracture the BN film but also for the extent of fracture. Furthermore, the critical load required to fracture a ceramic film on a substrate can be determined by measurements of the scratch width. The fracture and wear of BN films are discussed in greater detail in the next section.



(a) BN film on 440C stainless steel and uncoated 440C stainless steel.  
 (b) BN film on 304 stainless steel and uncoated 304 stainless steel.  
 (c) BN film on Ti and uncoated Ti.

Figure 16.—Mean contact pressure (yield pressure) as function of load for metallic substrates (sliding velocity, 12 mm/min; laboratory air).

Mean contact pressure (yield pressure)  $P$  during sliding may then be defined by  $P = W/A_s$ , where  $W$  is the applied load and  $A_s$  is the projected contact area given by  $A_s = \pi D^2/8$  (only the front half of the pin is in contact with the flat) [51,52].

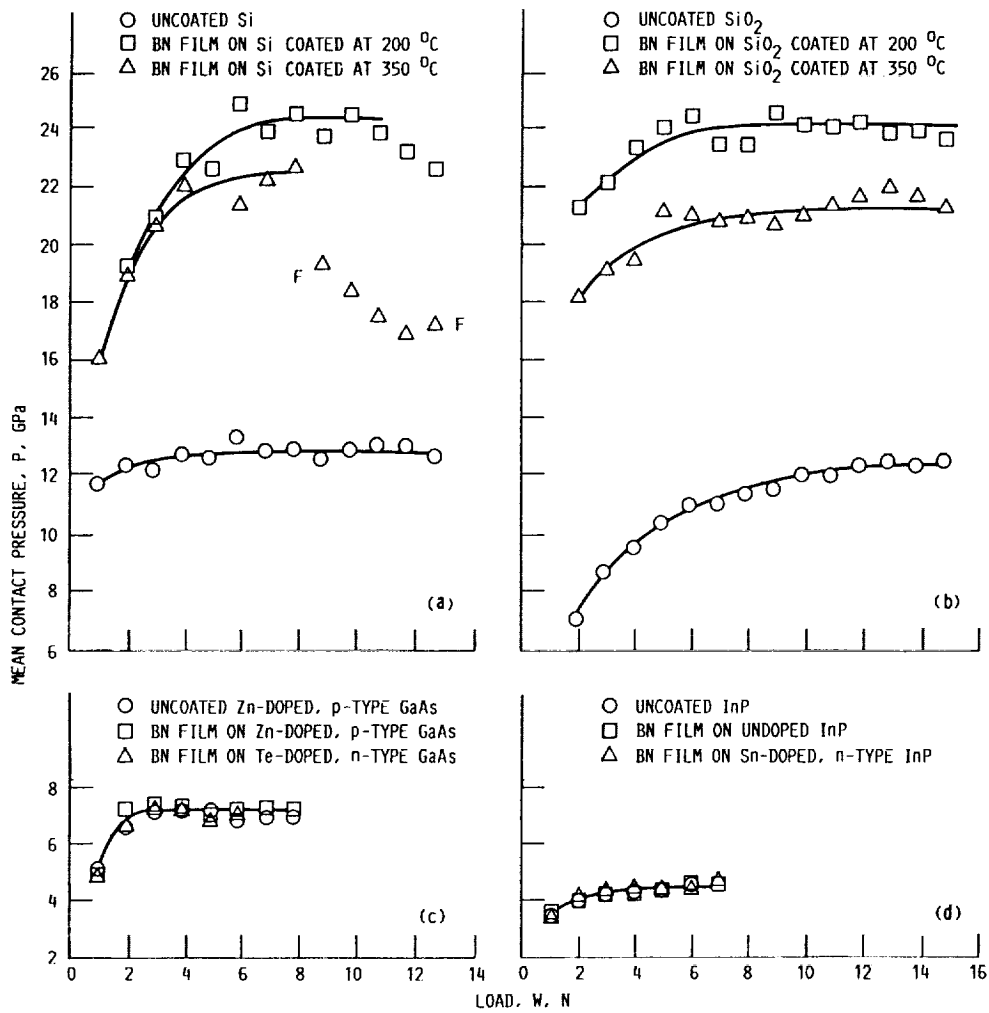
The mean contact pressure over the contact area gradually increased until the deformation passed to a fully plastic state, as presented in figure 16 for metallic substrates and in figure 17 for nonmetallic substrates. The mean contact pressure at a fully plastic state  $P_m$  is higher than but proportional to the measured Vickers hardness (tables II–IV).

The mean contact pressure of 440C stainless steel, 304 stainless steel, titanium, silicon, and  $\text{SiO}_2$  increased by a factor of up to 2 with the presence of BN films (figs. 16 and 17).

The mean contact pressures for BN films on doped GaAs and InP are the same as those for the uncoated surfaces of doped GaAs and InP (figs. 17(c) and (d)). Optical microscopic examination of the grooves on the BN films deposited on doped GaAs and InP substrates clearly revealed that the sliding action caused breakthrough of the film in the contact area. The breakthrough of the BN films was caused by poor interfacial adhesive bonds between the film and the substrate in and near the diamond contact region. The removal of the BN films induced direct contact of the diamond pin with the doped GaAs and InP substrates. It therefore resulted in no increase in the mean contact pressure of the doped GaAs and InP with the presence of BN films.

### Fracture and Wear

When a much higher contact pressure (due to highly concentrated stress in the contact area between the diamond and BN film) is provided, the sliding action produces visible microscopic cracking in the BN film. Scanning electron photomicrographs of a wear track on a BN film deposited on a 304 stainless steel substrate (fig. 18) reveal that both plastic deformation and fracture occurred in the BN film. The fracturing resulted from brittle cracks being generated, propagated, and then intersected in the BN film and at the interface between the BN film and the substrate. The backscatter photomicrograph (fig. 18(b)) reveals two different materials: (1) The dark areas in the photomicrograph show where the BN film stayed on the substrate and (2) the light areas show where the BN film fragments came off, revealing the 304 stainless steel substrate.



(a) BN film on Si and uncoated Si.  
 (b) BN film on SiO<sub>2</sub> and uncoated SiO<sub>2</sub>.  
 (c) BN film on GaAs and uncoated GaAs.  
 (d) BN film on InP and uncoated InP.

Figure 17.—Mean contact pressure (yield pressure) as function of load for nonmetallic substrates (sliding velocity, 12 mm/min; laboratory air; portion FF represents fractured scratch on BN film).

TABLE II.—CRITICAL NORMAL LOAD TO FRACTURE BN FILM IN SLIDING CONTACT AND SHEAR STRENGTH OF INTERFACIAL ADHESIVE BONDS

Substrate	Vickers hardness, $H_v$ , GPa		Mean contact pressure (yield pressure) at a fully plastic state, $P_m$ , GPa	Critical normal load, $W_c$ , N	Interfacial adhesive strength, $S$ , GPa	
	Substrate <sup>a</sup>	BN film <sup>b</sup>			$S = K \left( \frac{W_c P_m}{\pi R^2} \right)^{1/2}$	$S = \frac{2W_c}{\pi DR}$
440C stainless steel	7.1	10.2	12	11	0.77	0.68
304 stainless steel	2.5	4.3	4.1	7	.37	.29
Ti	2.6	3.4	3.3	8	.40	.30

<sup>a</sup>Hardness measuring load, 2 N.

<sup>b</sup>Hardness measuring load, 0.05 N.

TABLE III.—MEAN CONTACT PRESSURE (YIELD PRESSURE) OF AND CRITICAL NORMAL LOAD TO FRACTURE BN FILM COATED ON NONMETALLIC SUBSTRATE

Substrate and film	Mean contact pressure (yield pressure) at fully plastic state $P_m$ , GPa	Vickers hardness, <sup>a</sup> $H_v$ , GPa	Ratio $P_m/H_v$	Critical normal load, $W_c$ , N
Si coated with BN at 200 °C	24.0	18.8	1.28	7
Si coated with BN at 350 °C	21.9	17.5	1.25	7
SiO <sub>2</sub> coated with BN at 200 °C	23.9	---	---	3
SiO <sub>2</sub> coated with BN at 350 °C	21.2	17.2	1.23	3
Zn-doped, <i>p</i> -type GaAs coated with BN	7.15	5.72	1.25	3
Te-doped, <i>n</i> -type GaAs coated with BN	7.05	5.65	1.25	3
InP coated with BN	4.51	3.66	1.23	2
Sn-doped, <i>n</i> -type InP coated with BN	4.54	3.61	1.26	1

<sup>a</sup>Hardness measuring load, 0.05 N.

Scanning electron photomicrographs of a wear track on a BN film deposited on a 440C stainless steel substrate (fig. 19) reveal that the BN film deformed plastically during sliding at a load of 11 N. Permanent grooves were formed where the diamond began to slide. However, the sliding action also produced sudden gross flaking of the BN film. A large light area in the last half of the wear track (fig. 19(a)) is a fracture pit where the BN film was completely removed along the sliding direction of the diamond. This is confirmed by the backscatter photomicrograph (fig. 19(c)), which shows the light area to be the 440C stainless steel substrate. The fracturing and removal of the BN film from the 440C stainless steel substrate were caused by fracture of cohesive bonds in the BN film and interfacial adhesive bonds between the film and the substrate in and near the contact region with the diamond. The BN film was fractured and removed from the titanium substrate in a similar manner.

Investigators have detected released acoustic emissions when the intrinsic cohesive bonds in the ceramic coating film or the adhesive bonds between the film and substrate or both are broken and a new surface is created. The pattern and intensity of the acoustic emissions depend on the nature of the disturbance, that is, plastic flow, cracking, or flaking of fragments [53–56].

Figure 20 presents typical acoustic emission traces and friction force traces for a BN film deposited onto a nonmetallic substrate. When the BN film surface is brought into contact with a diamond pin under a small load (which is lower than the critical loads needed to fracture intrinsic cohesive bonds in the BN film and adhesive bonds between the film and substrate), no acoustic emission is detected (fig. 20(a)). The friction force trace at the same load (3 N) fluctuates slightly with no evidence of stick-slip behavior (fig. 20(b)). After the diamond has passed over the surface once, scanning electron microscopic examination of the wear track indicates that a permanent groove is formed in the BN film, much as occurs in metallic films under similar conditions [30,31]. However, no cracking of the BN film is observed with sliding.

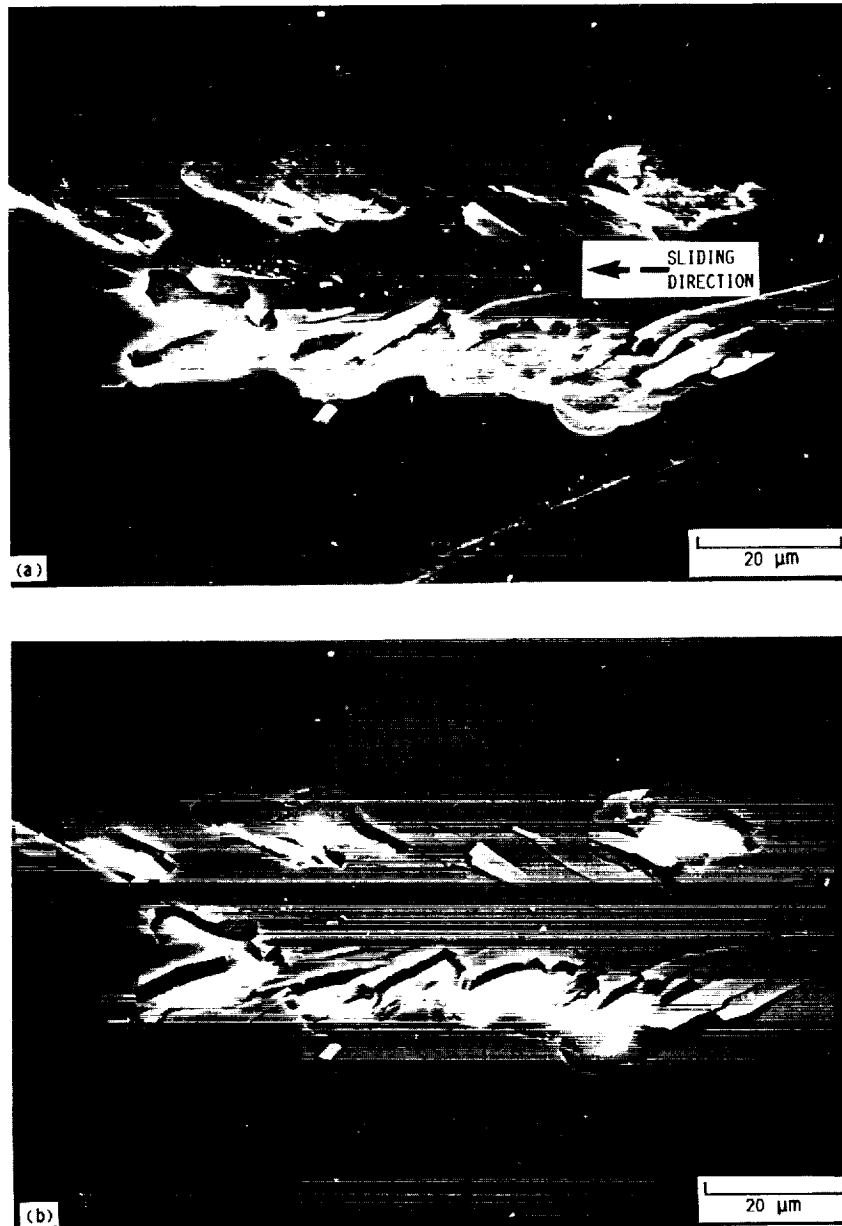
An increase in load to or above the critical loads required to fracture the BN film and the interfacial adhesive bonds between the film and the substrate results in a small amount of cracking in and near the plastically deformed groove. The acoustic emission trace detected at a load of 9 N indicates evidence of a fluctuating acoustic emission signal output (fig. 20(c)). Acoustic emission is observed when the sliding appears to involve small amounts of cracking in addition to plastic flow. Such acoustic emission is due to the release of elastic energy when cracks propagate in the BN film. The friction force trace measured at the load of 9 N is characterized by randomly fluctuating behavior, but only occasional evidence of stick-slip behavior is observed (fig. 20(d)).

TABLE IV.—MEAN CONTACT PRESSURE (YIELD PRESSURE) OF AND CRITICAL NORMAL LOAD TO FRACTURE NONMETALLIC MATERIALS

Material	Mean contact pressure (yield pressure) at fully plastic state $P_m$ , GPa	Vickers hardness, <sup>a</sup> $H_v$ , GPa	Ratio $P_m/H_v$	Critical normal load, $W_c$ , N
Si	12.6	9.89	1.27	5
SiO <sub>2</sub>	12.4	---	---	1
Zn-doped, <i>p</i> -type GaAs	6.94	5.61	1.24	2
Te-doped, <i>n</i> -type GaAs	---	5.68	---	—
InP	---	---	---	1
Sn-doped, <i>n</i> -type InP	4.35	3.49	1.25	1

<sup>a</sup>Hardness measuring load, 0.05 N.

ORIGINAL PAGE  
BLACK AND WHITE PHOTOGRAPH

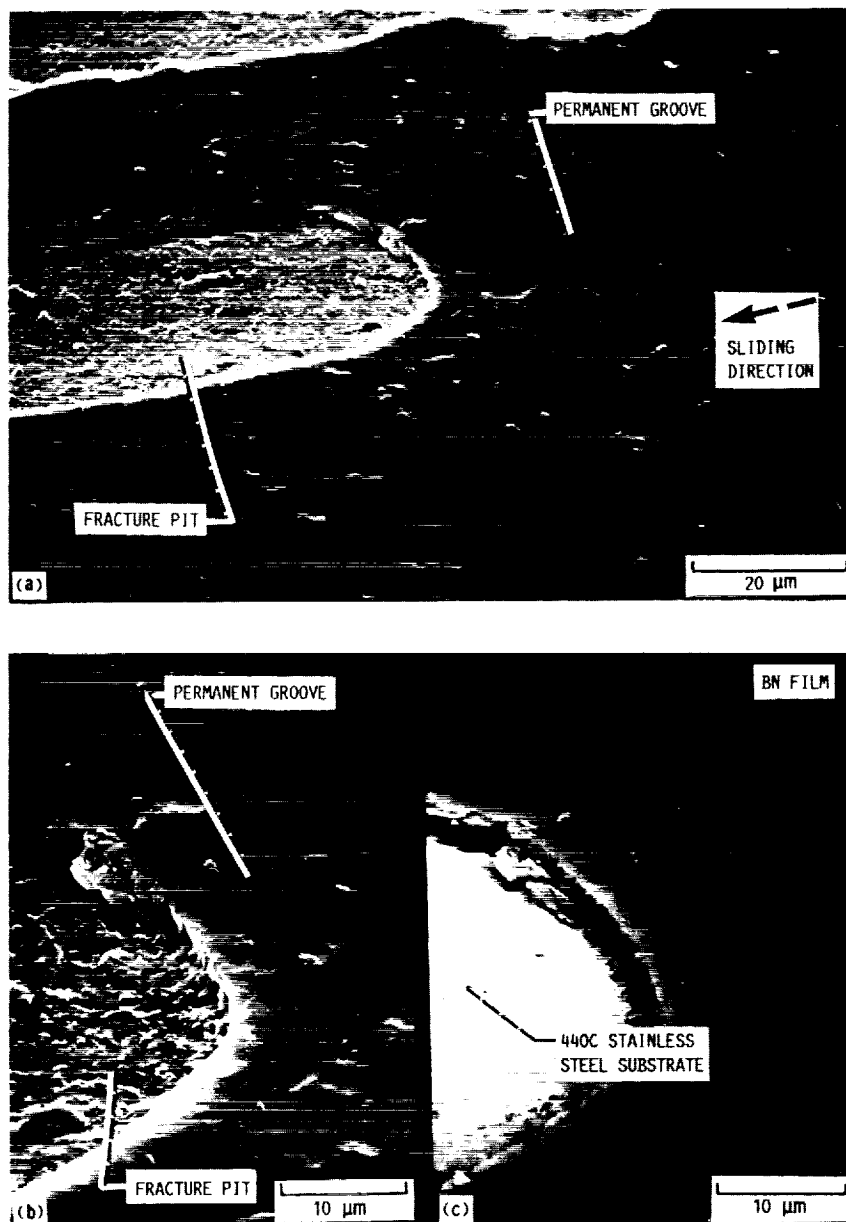


(a) Secondary electron image SEM.  
(b) Backscatter electron image SEM.

Figure 18.—Scanning electron microscope (SEM) photomicrographs of wear track on BN film surface generated by 0.2-mm-radius diamond pin (substrate, 304 stainless steel; load, 7 N; sliding velocity, 12 mm/min; laboratory air).

When a much higher load is applied to the BN film, the sliding action produces, in addition to plastic flow, locally gross surface and subsurface fracturing in the film and at the interface between the BN film and the substrate. In such cases the acoustic emission traces are primarily characterized by chevron-shaped peaks (fig. 20(e)), whereas the friction force is primarily characterized by a continuous, marked stick-slip behavior (fig. 20(f)).

The behavior of acoustic emission is related to that of the friction force. For example, at point I in figures 20(e) and (f), the diamond pin comes to rest until point II is reached. At point II, the pin is set into motion and slips, and will continue to move until point III is reached. At point II, acoustic emission is released because the slip action produces fracturing at the interface between the BN film and the substrate. At point III, the pin comes to rest again. Thus, fracture in the film and at the interface between the BN film and the substrate is responsible for the observed acoustic emission signal output and friction behavior. Acoustic and friction measurements of the critical load required to fracture a ceramic film on a substrate agree well with the critical loads detected by optical and scanning electron microscopy of the scratches.

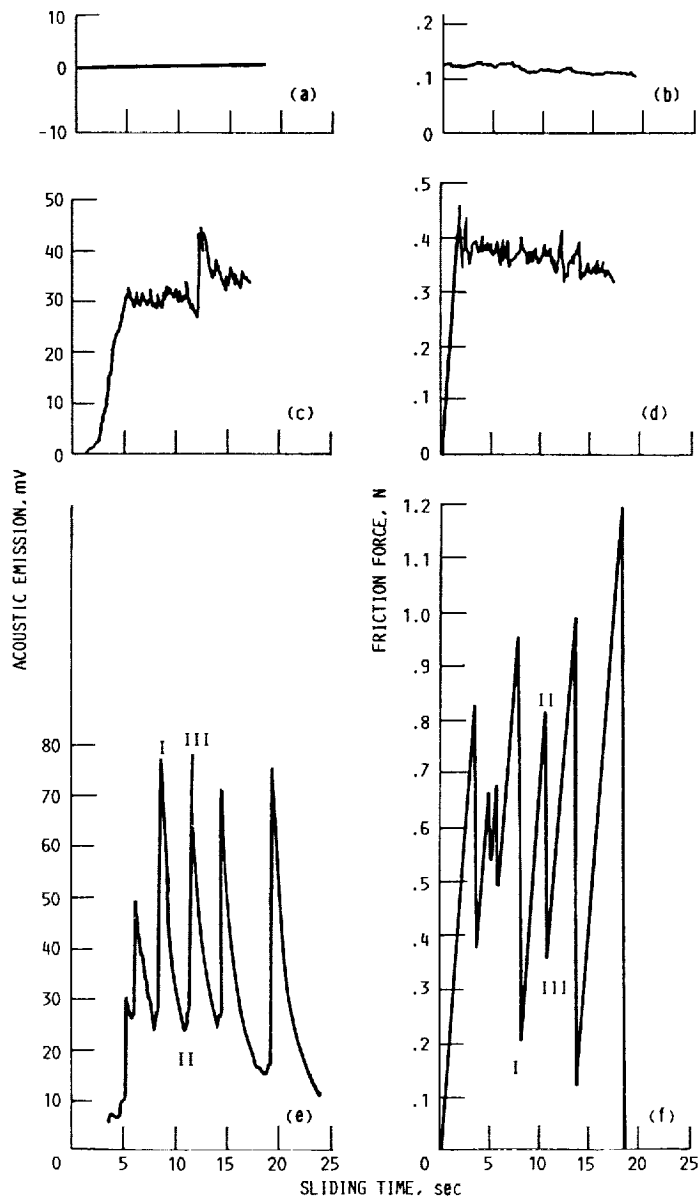


(a) Secondary electron image SEM (low magnification).  
 (b) Secondary electron image SEM (high magnification).  
 (c) Backscatter electron image SEM.

Figure 19.—Scanning electron microscope (SEM) photomicrographs of wear track on BN film surface generated by 0.2-mm-radius diamond pin (substrate, 440C stainless steel; load, 11 N; sliding velocity, 12 mm/min; laboratory air).

Figure 21 presents data on the critical loads required to fracture BN film and adhesive bonds between the film and metallic substrate as determined by acoustic emission and friction force measurements. The critical load to fracture is related to the hardness and strength of the metallic substrate. The harder the metallic substrate or the greater the strength of the substrate, the higher the critical load.

With uncoated silicon (table IV), the critical load to fracture cohesive bonds in the silicon was 5 N in sliding contact. With the BN film deposited on the silicon substrate, however, cracking occurred at a load of 7 N (table III). A similar trend was observed with good-quality BN films on SiO<sub>2</sub>, as well as with poorly adhered films on zinc-doped GaAs and undoped InP (tables III and IV). Thus, the BN film on the brittle, nonmetallic materials plays an important role in surface fracture. The presence of BN film is very effective in increasing the critical load needed to initiate fracture in nonmetallic material.



(a) No acoustic emission caused by diamond pin under small load, 3N.  
 (b) Friction force caused by diamond pin under small load, 3N.  
 (c) Acoustic emission caused by diamond pin under critical load, 9N.  
 (d) Friction force caused by diamond pin under critical load, 9N.  
 (e) Acoustic emission caused by diamond pin under much higher load, 12 N.  
 (f) Friction force caused by diamond pin under much higher load, 12 N.

Figure 20.—Typical acoustic emission traces and friction traces for BN film in contact with hemispherical diamond pin in laboratory air.

### Adhesion and Shear Strength

Interfacial adhesive bonds between the coating and the substrate or cohesive bonds in the BN coating or both were broken when critically loaded. For example, with 440C stainless steel and titanium, some of the interfacial adhesive bonds between the BN film and the substrate were generally weaker than the cohesive bonds in the BN film. The failed surface revealed the complete removal of the BN film from the 440C stainless steel surface (fig. 19) or the titanium surface.

On the other hand, with the 304 stainless steel, silicon, and  $\text{SiO}_2$  substrates, the interfacial adhesive bonds between the BN film and the substrate were generally stronger than the cohesive bonds in the BN film. The BN film first cracked when it was critically loaded. When a much higher load than the critical load was applied, the sliding action

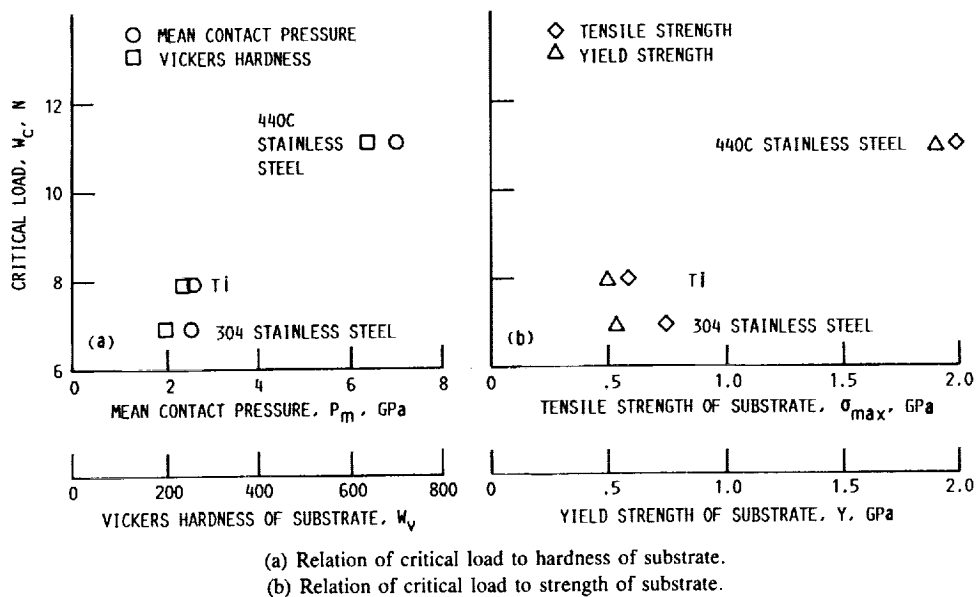


Figure 21.—Critical load needed to fracture BN film and interfacial adhesive bonds between film and substrate in sliding contact with hemispherical diamond pin in laboratory air (mean contact pressure is scratch hardness of substrate).

induced fracture of interfacial adhesive bonds between the BN film and the substrate, and the BN film fragments were partially removed from the substrate (e.g., fig. 18).

Although the failure modes observed with the BN films on the metallic and nonmetallic substrates were different, it is interesting to compare the adhesion strength of the interfacial bonds between the BN film and the substrate.

Benjamin and Weaver [57] derived the following expressions for scratch adhesion in terms of shearing stress  $S$  produced at the coating/substrate interface by the plastic deformation, the hardness of the substrate (mean contact pressure at fully plastic state  $P_m$ ), the critical load applied on the pin  $W_c$ , tip radius of the pin  $R$ , and the width of the resulting scratch  $D$

$$S = K \left( \frac{W_c P_m}{\pi R^2} \right)^{1/2} \quad (2)$$

$$S \approx \frac{2W_c}{\pi DR} \quad (3)$$

These relationships allow for the calculation of the shear strength (i.e., the adhesion strength of the interfacial bonds) [52,57]. The results are presented in tables II and V. The values of the critical loads were obtained and confirmed not only by optical and scanning electron microscopic examination of the scratches, but also by the acoustic emission technique. Table II reveals the strong correlation between the shear strength (i.e., adhesion strength) and the hardness of the substrate. The harder the metallic substrate, the greater the shear strength.

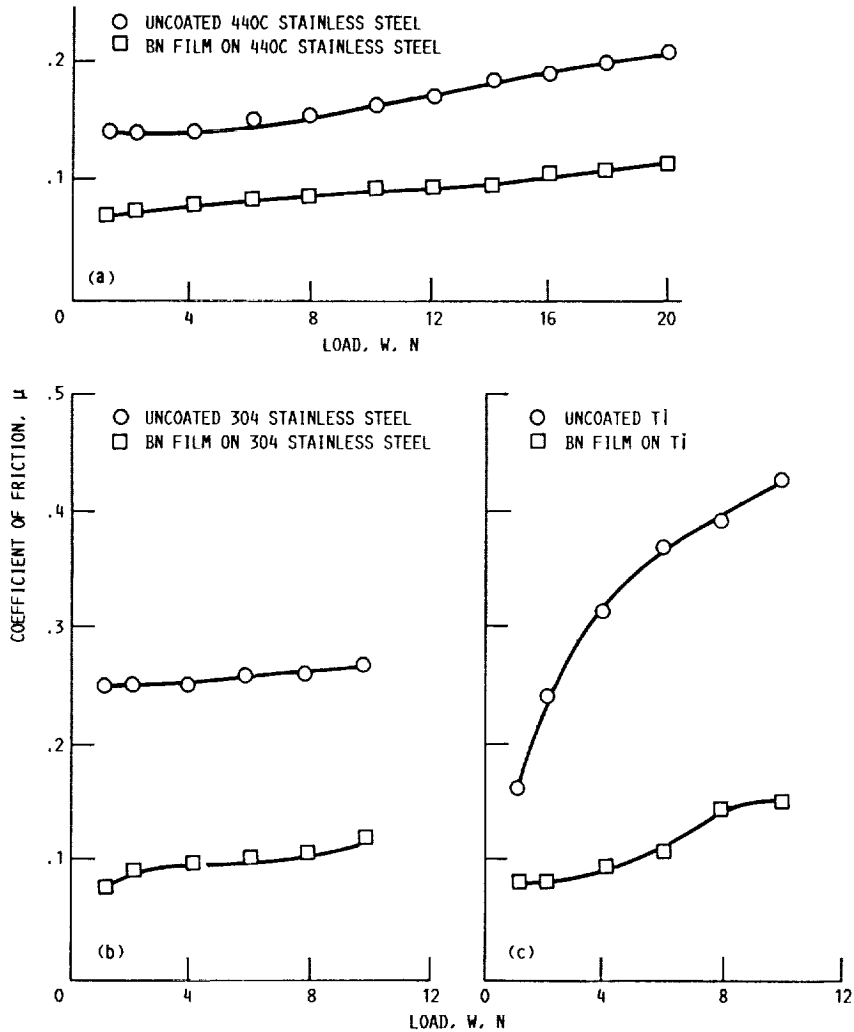
### Lubricating Effects of Boron Nitride Film

The coefficients of friction measured in laboratory air for BN films on the metallic and nonmetallic substrates are presented in figures 22 and 23, with comparative data for the uncoated metallic and nonmetallic materials. The friction resulted primarily from abrasion (plowing) of the diamond. The data presented in figures 22 and 23 indicate the marked difference in friction for presence or absence of BN films. The presence of BN films decreases adhesion and plastic deformation, and accordingly, friction. Thus, the ion-beam-deposited BN film can be effectively used as a solid lubricating film.

TABLE V.—CRITICAL NORMAL LOAD TO FRACTURE INTERFACIAL ADHESIVE BONDS BETWEEN BN FILM AND SILICON SUBSTRATE AND SHEAR STRENGTH OF INTERFACIAL ADHESIVE BONDS

Coating condition, <sup>a</sup> °C	Critical normal load, $W_c$ , N	Interfacial adhesive strength, $S$ , GPa	
		$S = K \left( \frac{W_c P_m}{\pi R^2} \right)^{1/2}$	$S = \frac{2W_c}{\pi DR}$
200	11	1.1	1.0
350	8	.91	.84

<sup>a</sup>Nominal temperature of substrate during ion-beam deposition.



(a) BN film on 440C stainless steel and uncoated 440C stainless steel.  
 (b) BN film on 304 stainless steel and uncoated 304 stainless steel.  
 (c) BN film on Ti and uncoated Ti.

Figure 22.—Coefficient of friction as function of load for metallic substrates (sliding velocity, 12 mm/min; laboratory air).

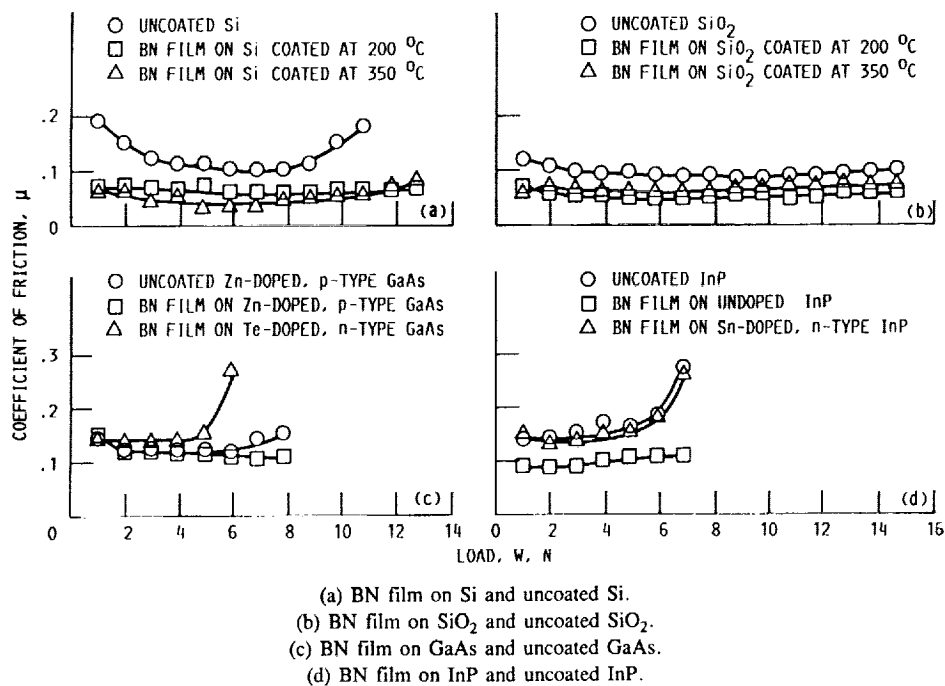


Figure 23.—Coefficient of friction as function of load for nonmetallic substrates (sliding velocity, 12 mm/min; laboratory air).

## CONCLUSIONS

Based on fundamental studies conducted on ion-beam-deposited boron nitride (BN) films grown on both metallic and nonmetallic substrates, the following comments can be made.

1. Ion-beam-deposited BN films are not completely amorphous but contain (to a small extent) hexagonal BN.
2. Both the sputter-cleaned surfaces and the bulk BN films are nonstoichiometric, with a boron-to-nitrogen (B/N) ratio of approximately 2, and contain small amounts of oxides and carbides in addition to BN.
3. Surface films on BN coatings affect their tribological behavior. For example, adsorbed carbon contaminants on a BN coating surface decrease both adhesion and friction, whereas oxygen, as a surface contaminant on metals in sliding contact with BN films, increases adhesion and friction.
4. For clean metal-to-BN contacts, strong bonds form between the materials, and the interfacial bonds are stronger than the cohesive bonds in the metal at a major part of the real area of contact. Adhesion and friction are strongly dependent on the ductility of the metals. Hardness of metals is of paramount importance to adhesion and friction, exceeding that of the surface energy of metals.

Adhesion, friction, surface energy, and hardness of a metal in contact with a BN film are all related to its shear modulus, which has a marked dependence on the electron configuration of the metal.

5. Boron nitride films, like metal films, deform elastically and plastically in the interfacial region between two solids in contact under load. Unlike metal films, however, when the contact stress exceeds a certain critical value, fracture can occur. The critical load to fracture is related to the hardness and strength of the substrates. The harder the substrate or the greater the strength of the substrate, the higher the critical load.

The critical load required to fracture a BN film on a substrate can be determined by measurements of the scratch width, acoustic emission, or friction as well as by optical or scanning electron microscopic examinations of the scratches.

6. The presence of BN films decreases adhesion and plastic deformation, and accordingly, friction. The BN films exhibited a capability for lubrication (low adhesion and friction) in both vacuum and air at atmospheric pressure.

## ACKNOWLEDGMENT

The author would like to thank John J. Pouch and Samuel A. Alterovitz, NASA Lewis Research Center, for providing the BN films deposited on the nonmetallic substrates.

## REFERENCES

1. Research Group on Wear of Engineering Materials: Friction, Wear, and Lubrication—Terms and Definition. O.E.C.D. Committee for Scientific Research, Delft, Netherland, 1966.
2. Sliney, H.E., Jacobson, T.P., Deadmore, D., and Miyoshi, K.: *Ceram. Eng. Sci. Proc.*, 1986, **7**, 1039.
3. Quinn, T.F.J.: *Wear*, 1984, **100**, 399.
4. Sutor, P.: *Ceram. Eng. Sci. Proc.*, 1985, **6**, 963.
5. Rice, R.W.: *Ceram. Eng. Sci. Proc.*, 1985, **6**, 940.
6. Buckley, D.H., and Miyoshi, K.: *Ceram. Eng. Sci. Proc.*, 1985, **6**, 919.
7. Kiser, J.D., Levine, S.R., and DiCarlo, J.A.: NASA CP-10003-SESS-1, 1987, **103**.
8. Sliney, H.E.: NASA CP-10003-SESS-1, 1987, **89**.
9. Brindley, P.K.: NASA CP-10003-SESS-1, 1987, **73**.
10. Buckley, D.H.: *Surface Effects in Adhesion, Friction, Wear, and Lubrication*. Elsevier, 1981, 245.
11. Czichos, H.: *Wear*, 1984, **100**, 579.
12. Halling, J., and Arnell, R.D.: *Wear*, 1984, **100**, 367.
13. Hintermann, H.E.: *Wear*, 1984, **100**, 381.
14. Schintlmeister, W., Wallgram, W., Kanz, J., and Gigl, K.: *Wear*, 1984, **100**, 153.
15. Miyoshi, K., and Buckley, D.H.: *Wear*, 1986, **110**, 295.
16. Buckley, D.H.: *ASLE Trans.*, **21**, 1978, 118.
17. Alterovitz, S.A., Warner, J.D., Liu, D.C., and Pouch, J.J.: *Proceedings of the Symposium on Dielectric Films on Compound Semiconductors*. V.J. Kapoor, D.J. Connolly, and Y.N. Wong, eds. Electrochemical Society, Pennington, 1986, 59.
18. Pouch, J.J., Alterovitz, S.A., and Warner, J.D.: NASA TM-87258, 1986.
19. Weissmantel, C.: *J. Vac. Sci. Technol.*, 1981, **18**, 179.
20. Shanfield, S., and Wolfson, R.: *J. Vac. Sci. Technol. A*, 1983, **1**, 323.
21. Motojima, S., Tamura, Y., and Sugiyama, K.: *Thin Solid Films*, 1982, **88**, 269.
22. Muraka, S.P., Cheng, C.C., Wang, D.N.K., and Smith, T.E.: *J. Electrochem. Soc.*, 1979, **126**, 1951.
23. Hyder, S.B., and Yep, T.O.: *J. Electrochem. Soc.*, 1976, **123**, 1721.
24. Liu, D.C., Valco, G.J., Skebe, G.G., and Kapoor, V.J.: *Proceedings of the Symposium on Silicon Nitride Thin Insulating Films*, V.J. Kapoor and H.J. Stein, eds., Electrochemical Society, Pennington, 1983, 141.
25. Miyamoto, H., Hirose, M., and Osaka, Y.: *Jpn. J. Appl. Phys. Part 2*, 1983, **22**, L216.
26. Wiggins, M.D., and Aita, C.R.: *J. Vac. Sci. Technol. A*, 1984, **2**, 322.
27. Adams, A.C.: *J. Electrochem. Soc.*, 1981, **128**, 1378.
28. Nakamura, K.: *J. Electrochem. Soc.*, 1985, **132**, 1757.
29. Miyoshi, K., Buckley, D.H., and Spalvins, T.: *J. Vac. Sci. Technol. A*, 1985, **3**, 2340.
30. Miyoshi, K., Buckley, D.H., Pouch, J.J., Alterovitz, S.A., and Sliney, H.E.: *Tribology—Friction, Lubrication and Wear*, **2**, Mechanical Engineering Publications, London, 1987, 621.
31. Miyoshi, K., et al.: *Surf. Coat. Technol.*, 1987, **33**, 221.
32. Tabor, D.: NASA CP-2300, 1983, **1**, 1.
33. Pepper, S.V.: *J. Appl. Phys.*, 1976, **47**, 2579.
34. Miyoshi, K., and Buckley, D.H.: *Ceram. Eng. Sci. Proc.*, 1983, **4**, 674.
35. Bowden, F.P., and Tabor, D.: *The Friction and Lubrication of Solids—Part II*. Clarendon Press, Oxford, 1964, 158.
36. Miyoshi, K., and Buckley, D.H.: *ASLE Trans.*, 1979, **22**, 79.
37. Gschneidner, K.A., Jr.: *Solid State Physics*, **16**, F. Seitz and D. Turnbull, eds., Academic Press, 1964, 275.
38. Tyson, W.R.: *Can. Metall. Q.*, 1975, **14**, 307.
39. Jones, H.: *Met. Sci. J.*, 1971, **5**, 15.
40. Miedema, A.R.: *Z. Metallk.*, 1978, **69**, 287.
41. Miyoshi, K., and Buckley, D.H.: *ASLE Trans.*, 1984, **27**, 15.
42. Tabor, D.: *J. Lubr. Technol.*, 1977, **99**, 387.
43. Rabinowicz, E.: *Friction and Wear of Materials*. John Wiley and Sons, 1965.
44. Miyoshi, K., Buckley, D.H., and Srinivasan, M.: *Am. Ceram. Soc. Bull.*, 1983, **62**, 494.
45. Miyoshi, K.: *Surf. Coat. Technol.*, 1988, **36**, 487.
46. Steijn, R.P.: *J. Appl. Phys.*, 1961, **32**, 1951.
47. Steijn, R.P.: *J. Appl. Phys.*, 1963, **34**, 419.
48. Steijn, R.P.: *Wear*, 1964, **7**, 48.
49. Steijn, R.P.: *ASLE Trans.*, 1969, **12**, 21.
50. DuFrane, K.F., and Glaeser, W.A.: NASA CR-72530, 1969.
51. Tabor, D.: *The Hardness of Metals*. Clarendon Press, Oxford, 1951.
52. Ahn, J., Mittal, K.L., and MacQueen, R.H.: *Adhesion Measurements of Thin Films, Thick Films, and Bulk Coatings*, K.L. Mittal, ed., ASTM Special Technical Publication 640, 1978, 134.
53. Hintermann, H.E.: *Wear*, 1984, **100**, 381.
54. Hintermann, H.E.: *Science of Hard Materials*, R.K. Viswanadham, D.J. Rowcliffe, and J. Gorland, eds., Plenum, 1983, 357.
55. Sekler, J., Steinmann, P.A., and Hintermann, H.E.: *Surf. Coat. Technol.*, 1988, **36**, 519.
56. Rickerby, D.S.: *Surf. Coat. Technol.*, 1988, **36**, 541.
57. Benjamin, P., and Weaver, C.: *Proc. R. Soc. London A*, 1960, **254**, 163.



# Report Documentation Page

1. Report No. NASA TM-102088		2. Government Accession No.		3. Recipient's Catalog No.	
4. Title and Subtitle Fundamental Tribological Properties of Ion-Beam-Deposited Boron Nitride Films			5. Report Date October 1989		
			6. Performing Organization Code		
7. Author(s) Kazuhisa Miyoshi			8. Performing Organization Report No. E-4850		
			10. Work Unit No. 506-43-11		
9. Performing Organization Name and Address National Aeronautics and Space Administration Lewis Research Center Cleveland, Ohio 44135-3191			11. Contract or Grant No.		
			13. Type of Report and Period Covered Technical Memorandum		
12. Sponsoring Agency Name and Address National Aeronautics and Space Administration Washington, D.C. 20546-0001			14. Sponsoring Agency Code		
15. Supplementary Notes This material will appear as a Chapter in Synthesis and Properties of Boron Nitride published by Trans. Tech. Publications, Aedermannsdorf, Switzerland.					
16. Abstract The adhesion, friction, and micromechanical properties of ion-beam-deposited boron nitride (BN) films are reviewed in this chapter. The BN films are examined in contact with BN metals and other harder materials. For simplicity of discussion, the tribological properties of concern in the processes are separated into two parts. First, the pull-off force (adhesion) and the shear force required to break the interfacial junctions between contacting surfaces are discussed. The effects of surface films, hardness of metals, and temperature on tribological response with respect to adhesion and friction are considered. The second part deals with the abrasion of the BN films. Elastic, plastic, and fracture behavior of the BN films in solid-state contact are discussed. The scratch technique of determining the critical load needed to fracture interfacial adhesive bonds of BN films deposited on substrates is also addressed.					
17. Key Words (Suggested by Author(s)) Boron nitride film Tribology Adhesion			18. Distribution Statement Unclassified - Unlimited Subject Category 27		
19. Security Classif. (of this report) Unclassified		20. Security Classif. (of this page) Unclassified		21. No of pages 24	22. Price* A03